



# Cardiovascular magnetic resonance imaging for structural heart disease

Yiling Situ<sup>1,2,3</sup>, Samuel C. M. Birch<sup>1</sup>, Camila Moreyra<sup>1</sup>, Cameron J. Holloway<sup>1,2,3</sup>

<sup>1</sup>St Vincent's Hospital Sydney, New South Wales, Australia; <sup>2</sup>St Vincent's Clinical School, University of New South Wales, Kensington, Australia;

<sup>3</sup>Victor Chang Cardiac Research Institute, Darlinghurst, Australia

*Contributions:* (I) Conception and design: CJ Holloway, Y Situ; (II) Administrative support: None; (III) Provision of study materials or patients: All authors; (IV) Collection and assembly of data: Y Situ, SCM Birch, C Moreyra; (V) Data analysis and interpretation: All authors; (VI) Manuscript writing: All authors; (VII) Final approval of manuscript: All authors.

*Correspondence to:* A/Prof Cameron J. Holloway, St Vincent's Hospital, 390 Victoria Street, Darlinghurst NSW 2010, Australia.

Email: camholloxford@gmail.com.

**Abstract:** Cardiovascular magnetic resonance (CMR) has increasingly become a powerful imaging technique over the past few decades due to increasing knowledge about clinical applications, operator experience and technological advances, including the introduction of high field strength magnets, leading to improved signal-to-noise ratio. Its success is attributed to the free choice of imaging planes, the wide variety of imaging techniques, and the lack of harmful radiation. Developments in CMR have led to the accurate evaluation of cardiac structure, function and tissues characterisation, so this non-invasive technique has become a powerful tool for a broad range of cardiac pathologies. This review will provide an introduction of magnetic resonance imaging (MRI) physics, an overview of the current techniques and clinical application of CMR in structural heart disease, and illustrated examples of its use in clinical practice.

**Keywords:** Cardiovascular magnetic resonance imaging (CMR imaging); cardiomyopathy; ischemic heart disease; structural heart disease

Submitted May 12, 2019. Accepted for publication Jun 10, 2019.

doi: 10.21037/cdt.2019.06.02

View this article at: <http://dx.doi.org/10.21037/cdt.2019.06.02>

## Introduction to magnetic resonance imaging (MRI)

The physics behind MRI is complex. MRI utilises proton excitation, decay, and net movements within alternating magnetic fields to generate images along different planes. The images are generated based on the magnetic resonance property of hydrogen protons within each tissue type, particularly water and fat. Each hydrogen nuclei contain an intrinsic magnetic field known as a magnetic moment (spin) which exerts an effect on its single proton (1). An external magnetic field is applied to align the spin (net magnetisation), while an additional magnetic field, known as the radiofrequency pulse, redirects the net magnetisation and causes the alignment to move away from the first magnetic field. The radiofrequency pulse can be altered to

control both the speed of rotational motion (precession) and the degree of rotation. Once the radiofrequency pulse is switched off, the net magnetisation quickly returns to equilibrium and the rate at which this occurs is known as relaxation. T1 and T2 are unique processes of relaxation and different tissue components have different relaxation times in T1 and T2 sequencing, thus, generating high resolution images that can delineate different tissue types. T1 and T2 signal changes along a gradient and time scale can further be represented in an absolute pixelated colour map to provide quantitative assessment of myocardial composition, known as cardiac mapping. Direct quantification in T1 and T2 mapping eliminates the need for reference tissue to determine alterations in other myocardial regions, allowing for accurate assessment of diffuse myocardial disease (2,3). T2\* mapping accounts for the inhomogeneities of T2

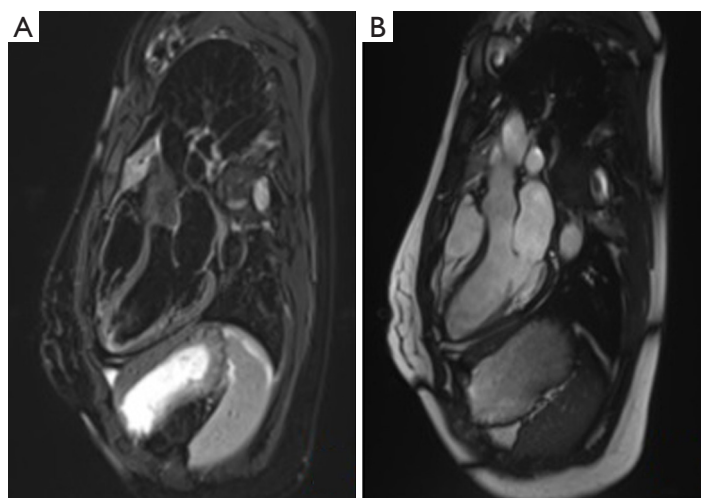


**Figure 1** Normal T2-weighted CMR in long axis. (A) Spin echo (black-blood sequence) and (B) gradient echo (white-blood sequence). CMR, cardiovascular magnetic resonance.

relaxation within tissues, and is useful for detecting iron composition in the myocardium. Furthermore, steady-state free precession (SSFP) utilises the ratio of T2/T1 relaxation rates to delineate tissue types with great spatial resolution.

## MR sequences and techniques

### *General techniques in CMR*

CMR is more complex than solid organ MRI, as it has to account for the variable orientation of the heart within the chest and the motion artefact involved in cardiac and respiratory motion. As such, a high degree of involvement from an experienced operator is important to adjust the orientation of imaging slices, appropriately choose CMR sequences based on clinical suspicion, and review image reconstruction.

The most commonly used technique to eliminate respiratory motion is breath-holding; generally asking the patient to hold their breath at end-expiration, as this position is more reproducible than end-inspiration. Most current MRI techniques can be completed within one breath hold. Cardiac motion, however, cannot be paused to allow adequate time for image acquisition. Continuous electrocardiographic (EKG) triggering is used to accurately time image acquisition by capturing the same phase within each cardiac cycle, during many heart beats, often at mid to end diastole when the heart is relatively motionless (4). However, EKG signals can be affected by rapidly changing

radiofrequency fields, and arrhythmias can interfere with cardiac motion (5). There are techniques to get around these issues, including ultrafast turbo (single-shot) acquisition techniques, which obtain images within one cardiac cycle at the expense of compromised image quality (6). Clinical CMR studies are generally performed at 1.5 Tesla (T), which is a measure of magnetic field strength, and has less artefact, including less cardiac gating artefact.

### *Static imaging for anatomy and tissue characterisation*

Static images in CMR can be obtained using turbo spin-echo (where blood appears black: black-blood sequence), gradient echo (blood appears white: white-blood sequence, see *Figure 1*) or inversion recovery. The high resolution static images are obtained as a “stack” of parallel slices taken over several cardiac cycles during patient breath holding. The basis of spin-echo relies on the radiofrequency pulse to align the net magnetization at  $90^\circ$  (excitation pulse) and then  $180^\circ$  (re-focusing pulse), followed by measurements of relaxation in T1 and T2 sequencing. The rapidly moving blood within the cardiac chambers acquire the initial excitation pulse, but moves out of the frame before the subsequent re-focusing pulse. This causes a void with no signal detection, thus creating the “black-blood” effect of spin-echo. This black-blood appearance creates high contrast between blood and myocardium (see *Figure 2*). Furthermore, different tissue types have different relaxation times in T1 and T2 sequencing which is particularly useful in highlighting

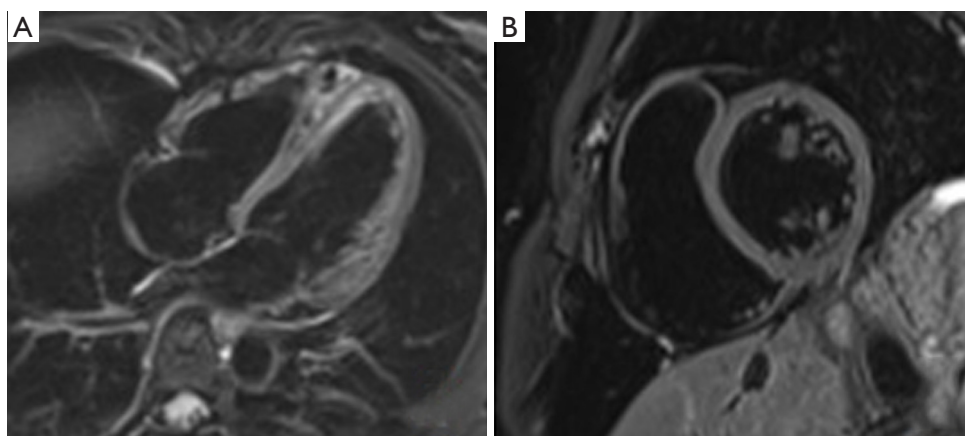


**Figure 2** T2-weighted imaging using spin echo black-blood sequencing. (A) Four-chamber view and (B) short-axis view.



**Figure 3** T1-weighted imaging at 1.5 T showing apical left ventricular aneurysm and associated LV thrombus (star) taken immediately after gadolinium administration.

cardiac anatomy, making spin-echo the choice for baseline images. In T1 sequencing, fat has fast relaxation time and appears bright, while water appears dark. Myocardium has intermediate relaxation time and can be separated from both fat and water. In addition, fat and water have different resonant frequency so using specific radiofrequency pulse to “saturate” fat can create a nulling signal where fat appears dark. This can confidently highlight fat components when compared to baseline images and can be used to separate pericardial fat from surrounding structures such as coronary vessels, cardiac tumours, and pericardial fluid (7).

Gadolinium-based agents further clarify cardiac structures. Gadolinium shortens T1 relaxation time and causes high signal enhancement in areas of increase uptake

or delayed washout. This is particularly useful in areas of inflammation depicted by accumulation of inflammatory cells, myocyte necrosis and remodelling with fibrotic tissue (8). Since chelated gadolinium is a large molecule, it accumulates easily in areas with increase extracellular volume fraction, and creates greater T1-shortening and high signal (9). Areas of increase gadolinium uptake thus appear brighter on T1-weighted imaging while low uptake such as thrombus (low signal) appears darker (see *Figure 3*). Increase gadolinium uptake occurs in myocardial inflammation which may signify diseases such as myocarditis, or infiltrative conditions like amyloidosis and sarcoidosis (10,11). In areas of fibrosis, the gadolinium takes longer to enter the cells and will have a longer wash-out period. Using inversion recovery sequence 10–30 minutes after injection of gadolinium, high signal areas of late gadolinium enhancement (LGE) can identify regions of fibrosis. T2-weighted imaging can be used additionally to confirm areas of active edema (high signal) and chronic fibrosis (low signal) when compared to pattern of LGE. In patients with hypertrophic cardiomyopathy, the extent of fibrosis identified through LGE has been significantly associated with sudden cardiac death (12). Using CMR, fibrosis has been identified in both ischemic and nonischemic cardiomyopathies, and is highly predictive of myocardial viability and can be used to guide clinical management.

#### *Cine imaging and phase velocity mapping for assessment of cardiac function and flow*

Cine imaging provides detailed functional assessment of

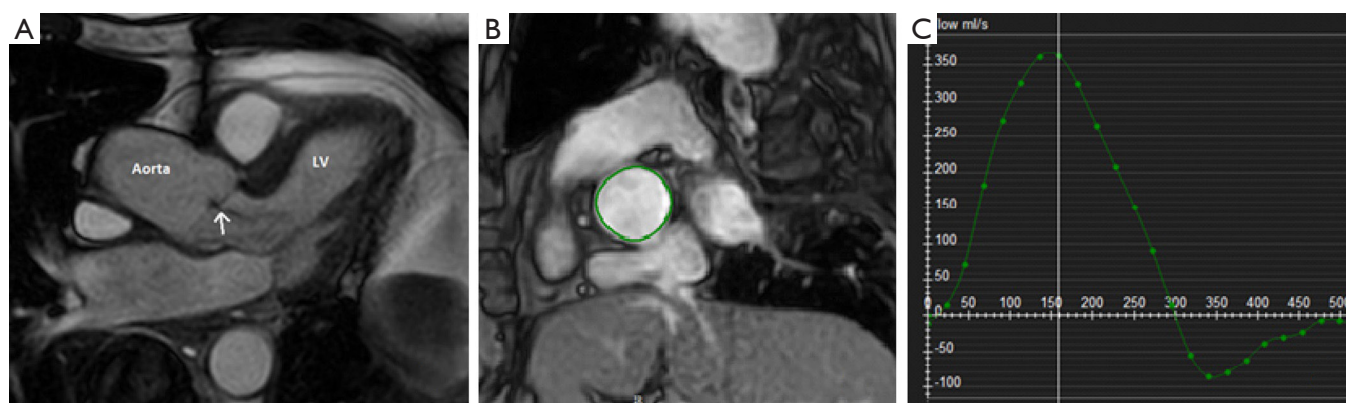


**Figure 4** Gradient pulse echo cine imaging using SSFP technique at 1.5 T demonstrating aortic regurgitation jet (arrow) in long-axis (A), through-plane phase-encoding across the aortic valve (B) and flow velocity mapping (C) where negative flow represents regurgitation.

the heart by visualising the movement of any part of the heart during the cardiac cycle, with clear definition of the endocardium and epicardium. Cine imaging captures multiple time points (known as cardiac phases) within the cardiac cycle. The images are taken over multiple cardiac cycles within one breath-hold and the same cardiac phases of each cardiac cycle are reconstructed together to create a high resolution image corresponding to that cardiac phase (1). When these images are replayed chronologically, it creates a “movie[cine]” of the functional motion of the heart. Cine imaging provides detailed visualisation of global and regional myocardial function, and using LV contouring of the myocardium at different cardiac phases can provide a detailed estimation of ejection fraction (13,14). This has been particularly useful in assessing right ventricular volume and function using short-axis cine stacks (15,16).

Gradient echo sequences are used for cine imaging. This allows for tracking of proton position because there is a unique radiofrequency pulse strength at different points along the gradient. Gradient echo uses an excitation radiofrequency pulse but not a refocusing pulse so there is no spin-out effect from moving blood. As the blood is constantly magnetised as it moves along the gradient, it creates a high signal “bright blood” contrast. The two main types of gradient echo pulse sequence used in cine imaging are spoiled gradient echo and balanced steady state free precession (SSFP). Spoiled gradient echo such as Fast Low Angle SHot (FLASH) uses rapid radiofrequency pulses to interfere with the previous radiofrequency pulse, causing partial saturation in static structures that remain within the imaging frame. Flowing blood, however, is only exposed to one radiofrequency pulse as it moves into the imaging

frame, thus providing high signal (inflow effect) compared to surrounding structures. SSFP uses timed successive radiofrequency signals to saturate the tissue and then measure the T2/T1 relaxation ratios to generate contrast images. In valvular disease, regurgitation jets of magnetised blood that returns to the previous imaging frame will have different radiofrequency exposure and saturation, thus appear darker than surrounding forward moving blood (see *Figure 4*).

Phase velocity mapping can be added to cine imaging (phase-encoded) to assess blood flow. In-plane (parallel to the tissue movement) and through-plane (perpendicular to the tissue movement) can be used to assess volume across a cross-sectional area and the velocity of the flow (see *Figure 4*). Moving blood accumulates different strengths of radiofrequency pulses as it moves along the gradient. Measuring the ultimate strength of the proton signal and the time interval between the gradient positions will directly correlate with velocity. Faster moving tissue will thus accumulate higher signal and move further along the gradient. These flow mapping techniques can be used to visualise blood flow across a valve including stenosis and regurgitation, blood flow velocities through true and false vessel lumens, and quantitative flow across shunts. The combination of cine imaging and flow mapping can provide detailed information about cardiac volumes and function.

### *MR angiography (MRA)*

MRA has been widely used for the assessment of larger vessels, including the thoracic aorta, carotid arteries, peripheral vasculature, renal arteries and intracranial vessels.

The non-invasive method provides excellent visualisation of vessel lumen, vessel trajectory, and origin of branches. In particular, 3D SSFP has been shown to be non-inferior to gold-standard CT angiogram for characterisation of the aorta (13,17).

Contrast-enhanced (CE) and non-contrast enhanced (NCE) sequences have been used in MR angiography. CE MRA is preferred as it shortens imaging time and provide better delineation of vessel structures. However, it relies heavily on precise tracking of the gadolinium-based contrast through the vessels. NCE MRA uses the basic principles of gradient echo and flow mapping to assess movement of blood and other particles within the lumen. These include time-of-flight, balanced steady-state free precession, and phase-contrast (PC) techniques which uses selective radiofrequency saturation pulse, T2 and T1 relaxation ratios, and bipolar velocity gradients respectively, to differentiate stationary structures from moving blood pool (18).

MRA of the coronary vessels is limited by cardiac and respiratory motion with poor spatial resolution. While Kim *et al.* (19) demonstrated high sensitivity and negative predictive value using MRA in assessing left main coronary artery disease and triple-vessel disease, MRA of the coronary arteries remains challenging and limited to clinical research. This is owing to the small size of coronary vessels, its proximity to the cardiac chambers, cardiac and respiratory motion, and prolonged scan time which all add to image quality degradation, ghosting artefact, and difficulty delineating the path and lumen characterisation of the vessels. As such, MR angiography of the coronary vessels is not used commonly in clinical practice and is not used diagnostically.

### **Perfusion imaging**

Early myocardial ischemia is reflected by subendocardial hypoperfusion deficits, while late changes include transmural ischemia, EKG changes, and clinical symptoms of chest pain. Traditionally, single-photon emission computed tomography (SPECT) have been used to assess perfusion abnormalities but the disadvantage lies in radiation exposure, and lack of specificity to subendocardial regions. Increasingly, CMR have been used to assess myocardial perfusion, especially when it has multiparametric properties to assess tissue characterisation and cardiac function in one scan (20,21).

Following the administration of intravenous gadolinium,

imaging is performed during the first-pass (perfusion of the myocardium) of gadolinium over 40–50 heart beats. Images are obtained both at rest, and after pharmacological stress, usually with adenosine or dipyridamole (22). Comparison between rest and stress images can identify any reduction in peak signal intensity or a delay to reach peak intensity, suggestive of myocardial hypoperfusion. Particularly, myocardial perfusion reserve (MPR) defined as the ratio of myocardial blood flow between rest and stress is an important indicator of ischemia (23). CMR perfusion techniques can undergo both visual and quantitative analysis. Epicardial and endocardial borders are outlined and divided into multiple segments. Signal intensity is calculated using software algorithms and quantitative measure of perfusion is obtained for every segment of myocardium (24). Cardiac synchronisation and ultra-fast T1-weighted gradient echo are used to obtain images of 2–3 mm<sup>2</sup> resolution, which can differentiate epicardial from endocardial perfusion. More advanced techniques such as Broad-use Linear Acquisition Speed-up Technique (k-t BLAST) and sensitivity encoding (k-t SENSE) uses parallel imaging techniques with multiple receiver coils simultaneously to improve spatial and temporal resolution to <2 mm<sup>2</sup> (25).

Multiple large scale studies have demonstrated superiority of CMR perfusion compared to SPECT for detection of myocardial ischemia, and reduction in unnecessary angiography (26–28). Additionally, cardiac ischemia can be further assessed by measuring global longitudinal strain whereby Romano *et al.* (29) demonstrated a significant relationship between global longitudinal strain > -19% and major adverse cardiovascular events in patients undergoing stress CMR.

### **CMR in clinical practice**

#### ***The assessment of cardiac mass, volumes and function for structural heart disease***

CMR provides accurate measurements of cardiac volumes and systolic function using cine imaging and myocardial contouring. Steady-state free precession imaging along the horizontal long axis, vertical long axis, and left ventricular outflow tract provide detailed anatomy of the heart. Short axis cine images are planned from these three planes and used for functional assessment (30). Using advanced software and manual contouring of the epicardium and endocardium at end diastole and end systole, assessment

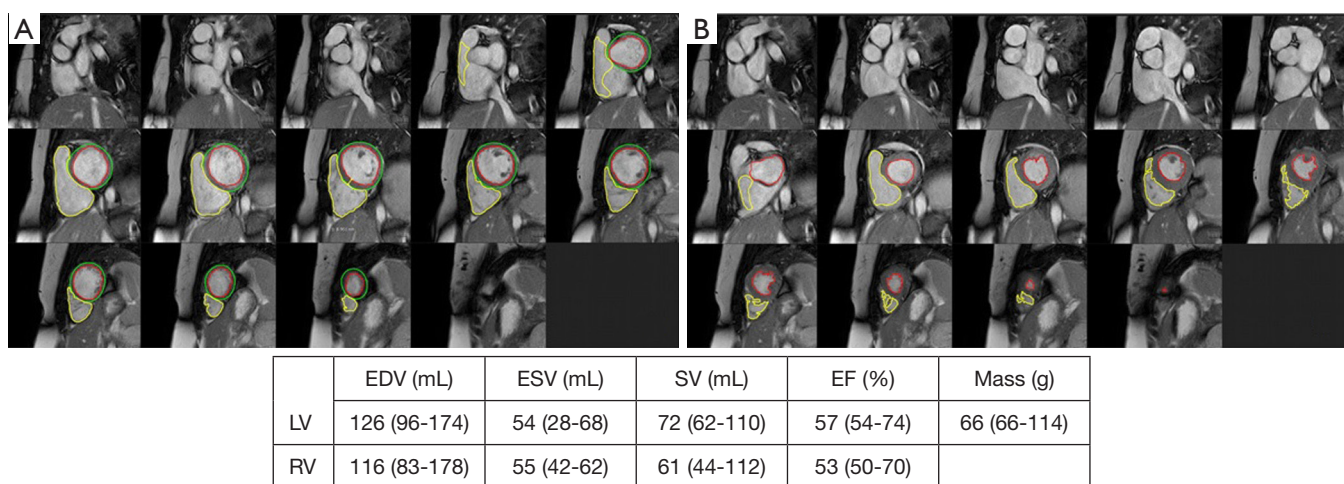


**Figure 5** Gradient pulse echo cine imaging with SSFP at 1.5 T and LV contouring in end diastole (A) and end systole (B) to assess left and right ventricular function with calculated end diastolic volume (EDV), end systolic volume (ESV), and ejection fraction (table).

of end diastolic volume, end systolic volume, myocardial mass, and ejection fraction can be performed with high accuracy (Figure 5) (16). This provides valuable structural information to assist clinical diagnosis and management. Furthermore, flow velocity mapping is commonly used to qualitatively and quantitatively assess blood flow across valves and shunts to provide further information.

### Cardiomyopathies

CMR is useful in assessing patients with heart failure or at risk of heart failure. Various CMR modalities are useful in diagnosing non-ischaemic causes of heart failure, as well as differentiating these causes. These CMR modalities include cine images to assess cardiac structure and function and tissue characterisation techniques. Late gadolinium enhancement, T1-mapping, T2-mapping, and T2\*-mapping have been used for tissue characterisation and are useful in determining the presence of non-ischaemic cardiomyopathy, the type of non-ischaemic cardiomyopathy, the extent and severity of disease, prognosis, and risk stratification (31). CMR is of particular utility in several non-ischaemic cardiomyopathies, including genetic cardiomyopathies (some forms of dilated cardiomyopathy, hypertrophic cardiomyopathy, and arrhythmogenic cardiomyopathy), autoimmune/inflammatory cardiomyopathies, and infiltrative cardiomyopathies (such as cardiac sarcoidosis, Fabry's disease, and cardiomyopathy associated with iron deposition) (31).

CMR is a useful modality in the diagnosis of dilated cardiomyopathy (DCM) which is a non-ischaemic cardiomyopathy that may be genetic or non-genetic in origin. It may be a final common pathway for a variety of pathological processes, such as drug/toxin exposure, acute myocarditis, and peripartum cardiomyopathy (32). DCM is characterised by left ventricular or biventricular dilatation and systolic impairment in the absence of abnormal loading conditions or significant coronary artery disease (32). Tissue characterisation modalities can assist in the diagnosis of DCM, for example, if mid-mural LGE is present, as opposed to the subendocardial enhancement typical of ischaemic cardiomyopathy. CMR can also determine the acuity of DCM by assessing for edema and fibrosis using T2-weighted and LGE sequences. The burden and distribution of fibrosis, if present, can consequently stratify patients of the risk of life-threatening arrhythmias (31).

Hypertrophic cardiomyopathy (HCM) is the most common cardiomyopathy with a genetic aetiology (33). CMR is of benefit in assessing patients with suspected or proven HCM by assessing morphology including quantification of maximal wall thickness, asymmetry of wall thickness, location of maximal wall thickness, and evidence of obstruction (Figure 6). Cine imaging along multiple planes can further assess biventricular systolic function, strain, and left ventricular outflow tract obstruction. The presence and extent of fibrosis, maximal wall thickness, and/or presence of left ventricular outflow tract obstruction are valuable information for risk stratification and guide

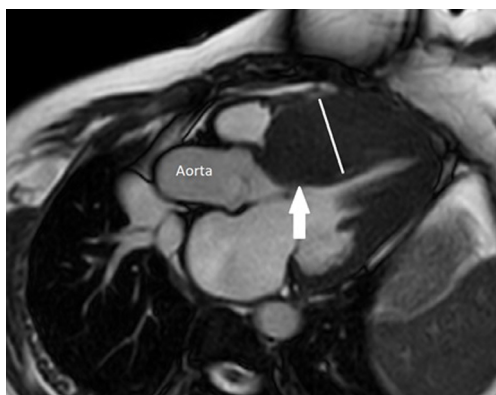


**Figure 6** Gradient echo with SSFP at 1.5 T showing hypertrophic cardiomyopathy with asymmetrical wall thickening (white line) and left ventricular outflow tract obstruction (arrow).

clinical management. CMR can further characterise the composition of the myocardium to provide diagnostic information for potential differential diagnoses including athlete's heart, hypertensive heart disease, valvular heart disease, and infiltrative cardiomyopathies (33).

CMR is an important alternative to cardiac biopsy in the diagnosis of cardiac amyloidosis. It has been reported to have approximately 100% sensitivity and 80% specificity for diagnosis of cardiac amyloidosis (34). LGE patterns on CMR in patients with cardiac amyloidosis are variable, and inversion times to null the myocardium are also variable in these patients. A global subendocardial circumferential pattern (that is generally arc shaped or annular and does not correspond to a particular coronary artery territory) of LGE has been reported as being the most frequent pattern observed in patients with biopsy-proven cardiac amyloidosis (35). Other patterns of LGE in cardiac amyloidosis include a zebra pattern of subendocardial and subepicardial fibrosis and a diffuse homogeneous enhancement (T1-mapping may assist in detection of this pattern) (35).

Arrhythmogenic cardiomyopathy (previously known as arrhythmogenic right ventricular cardiomyopathy) is a genetic cardiomyopathy that may involve both ventricles, but generally has its predominant effect on the right ventricle (36). A commonly used set of diagnostic criteria for this condition (37) includes several CMR features as major criteria for diagnosis. These criteria include regional right ventricular akinesia, dyskinesia, or dyssynchronous right ventricular contraction and one of the following criteria (end diastole): right ventricular end-diastolic volume/BSA  $>110$  mL/m<sup>2</sup> (male) or  $\geq 100$  mL/m<sup>2</sup> (female), or right ventricular

ejection fraction  $\leq 40\%$ . Tissue characterisation modalities are often not sensitive or specific enough to guide diagnosis of arrhythmogenic cardiomyopathy, because the fibrofatty infiltration present in this condition may not result in a readily seen area of LGE and because the presence of right ventricular LGE may be seen in other conditions (36).

CMR is also of benefit in the diagnosis of various inflammatory and infiltrative cardiomyopathies, such as cardiac sarcoidosis, cardiomyopathies related to other systemic autoimmune conditions, Fabry's disease, and iron deposition cardiomyopathy. Tissue characterisation modalities are of particularly utility in diagnosing these conditions, for example, unique distribution of LGE in cardiac sarcoidosis and other autoimmune cardiomyopathies, T1 mapping in Fabry's disease, and T2\* relaxation times in iron deposition cardiomyopathy (31).

### *Ischemic heart disease*

CMR allows accurate identification of cardiac anatomy, bi-ventricular function, viability, and myocardial perfusion, so has been broadly applied to the assessment of ischemic heart disease (38). Moreover, it can differentiate acute and chronic infarction from other causes of chest pain, including peri-myocarditis and aortic dissection (39).

In acute myocardial infarction (MI), a short tau inversion recovery sequence (T2-weighted) is performed to assess edema secondary to myocardial injury (38). Edematous myocardium displays increased signal intensity (bright), which can be detected as early as 30 minutes from symptom onset. It represents the ischemic area at risk (AAR), which is a significant determinant of infarct size and clinical outcome. This tissue response has been shown to increase the risk of adverse cardiovascular events, irrespective of revascularization (40). Early coronary reperfusion strategies reduce mortality by increasing the size of salvaged myocardium, defined as the proportion of AAR that does not become necrotic which is shown as late gadolinium enhancement (41,42).

Despite successful reperfusion of patients with ST-segment elevation myocardial infarction (STEMI), there may be a "no-reflow" phenomenon with absent or inadequate distal myocardial flow on coronary angiography. On CMR it is identified as microvascular obstruction (MVO) or intramyocardial hemorrhage (IMH). The former is shown with LGE as a region of hypo-enhancement within the hyper-enhanced area infarct zone (Figure 7) (43,44). The latter can easily be detected as a dark core on T2-weighted images.

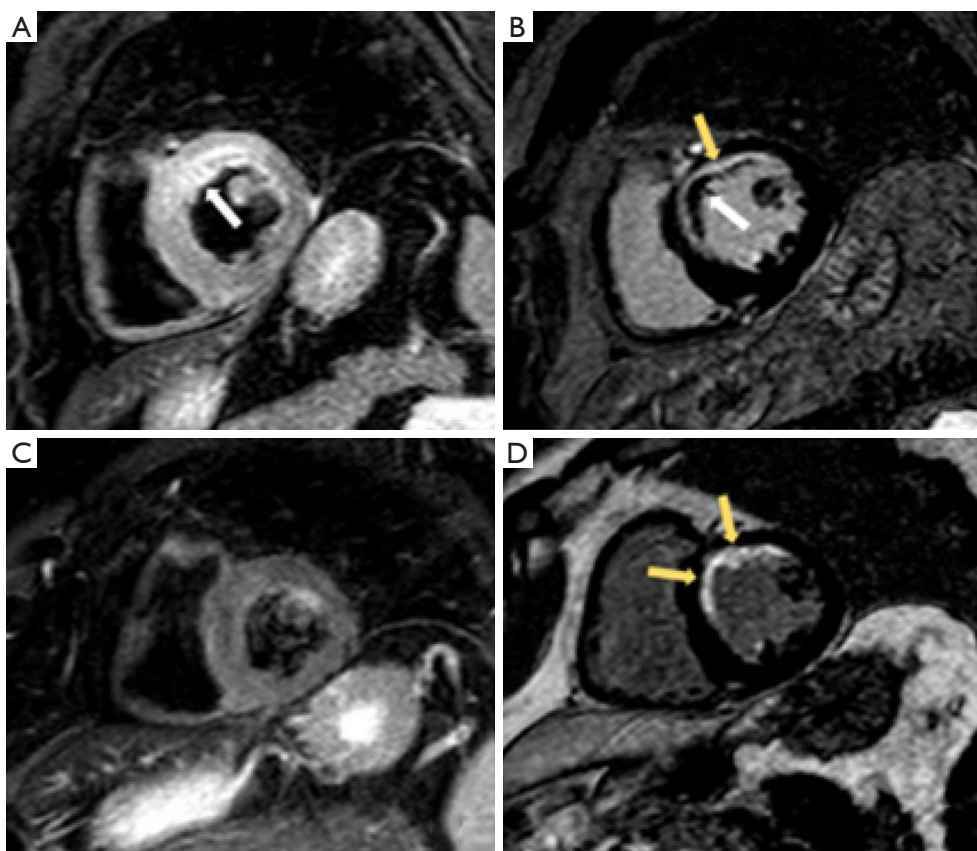


**Figure 7** Evolutionary changes of myocardial infarction. (A) Short-axis T2-weighted short tau inversion spin echo imaging show edema of the inflamed myocardium in the anteroseptal wall (white arrow). (B) Short-axis phase-sensitive inversion recovery (PSIR) sequence reveals presence of myocardial infarction (MI, upper arrow) with large area of late microvascular obstruction (LMVO, lower arrow); (C) short-axis T2-weighted sequence 5 months after MI, with no evidence of edema; (D) short-axis PSIR illustrating the MI scar (arrows), without evidence of LMVO.

Both are associated with poor prognosis (40).

In chronic ischemic heart disease, CMR has become the gold standard method for detecting myocardial scar (45). LGE with hyperintense signals are prominent in infarcted myocardium, and this can extend from the subendocardium to epicardium with transmural fibrosis (*Figure 8*). While CMR provide prognostic information, it also offers an assessment of myocardial viability (40). The likelihood of functional recovery post-revascularization becomes evident when at least 50% of the myocardium thickness is viable (46,47).

Compared to other non-invasive functional tests such as exercise stress echocardiography or nuclear imaging, CMR provides a substantially better temporal and spatial resolution which translates in better sensitivity, specificity, positive and negative predictive values for assessing

myocardial ischemia, without the limitations associated with poor echo windows (28,48,49).

#### *Valvular heart disease*

CMR techniques provide information on valvular pathology, with recent developments in this area. Assessment of valve structure and function is possible using CMR, including valve leaflets, valve tumours, and, less so, endocarditis (50). Cine images using bright-blood SSFP can be used, as can T1 and T2 weighted turbo-spin echo (black-blood technique) (51). Valvular areas by planimetry can also be assessed using CMR (50). Quantitative measures of aortic and pulmonary valvular functions can be assessed using flow velocity mapping with cine SSFP. However, the less rigid tricuspid and mitral valves are prone to motion artefact and



**Figure 8** Vertical long axis late gadolinium image at 1.5 T, acquired 10 minutes post-gadolinium administration demonstrating wall thinning and 50% to 75% transmural LGE in the mid to apical left ventricle (arrow) consistent with previous left anterior descending infarction.

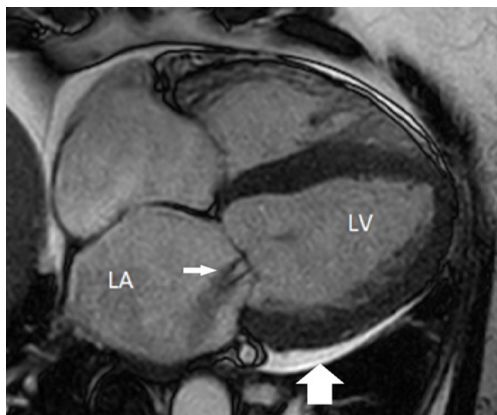


**Figure 9** 1.5 T gradient pulse echo with SSFP showing mitral regurgitation (small arrow) into a dilated left atrium. A small pericardial effusion (large arrow) also noted.

their quantitative function is assessed indirectly through volume changes in the corresponding ventricular inflow and outflow (*Figure 9*). Ventricular volumes, atrial size, and ventricular wall thickness can be indicators of severity of valvular pathology (51).

2D phase contrast flow imaging can provide useful information relevant to valve function and pathology (52). Assessment of peak velocity, peak pressure gradient, and regurgitant volume are possible with 2D phase contrast flow imaging, assisting in the evaluation of valvular stenosis and regurgitation (50). Flow visualization of venae contracta and regurgitant jets is also feasible with CMR (51). Accurate placement of the 2D acquisition near the level

of the aortic valve in the assessment of the aortic stenosis remains difficult, and the peak velocity in aortic stenosis is often underestimated on CMR (52). 4D flow MRI is a more recent technique and can provide comprehensive information on blood flow dynamics. Difficulties with assessing aberrant jets in aortic stenosis are more likely to be overcome with 4D flow MRI than 2D phase contrast flow imaging (52).

However, as the cine images are taken over multiple cardiac cycles, spatial resolution is reduced and accurate assessment of small, highly mobile structures can be difficult. Echocardiography in real-time remains useful for assessing valvular anatomy and function in clinical practice.

### *Pericardial disease*

CMR is globally the most appropriate technique to evaluate the pericardium. It provides information about pericardium morphology and surrounding structures; tissue characterization, evaluation of pericardial mobility and fusion of pericardial layers (53).

To visualize the hearts anatomy, the pericardium, and mediastinal structures, black-blood T1-weighted spin-echo sequence and bright-blood cine SSFP imaging are often used (*Figure 10*) (54,55). A normal pericardium appears as a smooth and curvilinear structure with an intermediate-to-low signal, which is surrounded by high-signal epicardial and mediastinal fat. Normal pericardial thickness is less than 2 mm while greater than 4 mm of thickening is considered abnormal (56). T2 weighted spin-echo imaging, preferably performed by using a short-tau inversion recovery sequence provides better visualisation of pericardial fluid and/or adjacent myocardial inflammation in patients with inflammatory pericarditis (*Figure 11*) (57,58). LGE can diagnose the extent of myo-pericardial inflammation/necrosis (59). The sensitivity of pericardial LGE for detection of pericardial inflammation is high with reported values of 95% (60).

Other pericardial diseases, such as constrictive pericarditis, can be assessed using real-time, free breathing sequences to evaluate constrictive physiology. During pericardial constriction, right and left ventricular pressures are equalized leading to diastolic interventricular septal displacement towards the left ventricle during inspiration when venous blood inflow to the right ventricle is increased (see *Figure 12*) (61). There is tethering and restricted ventricular expansion adjacent to thickened areas, which can be assessed with MR tagging techniques. Nonetheless,

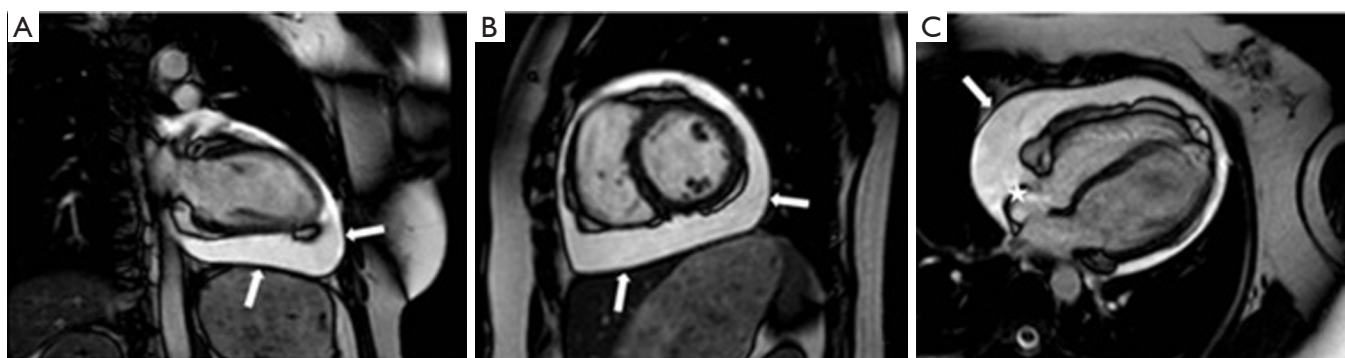


**Figure 10** SSFP imaging of a severe-sized pericardial effusion that is homogenously high in signal (white arrows). (A) Vertical long-axis; (B) short-axis through the mid-cavity level of the left ventricle; (C) horizontal long-axis shows collapse of the right atrium during diastole.

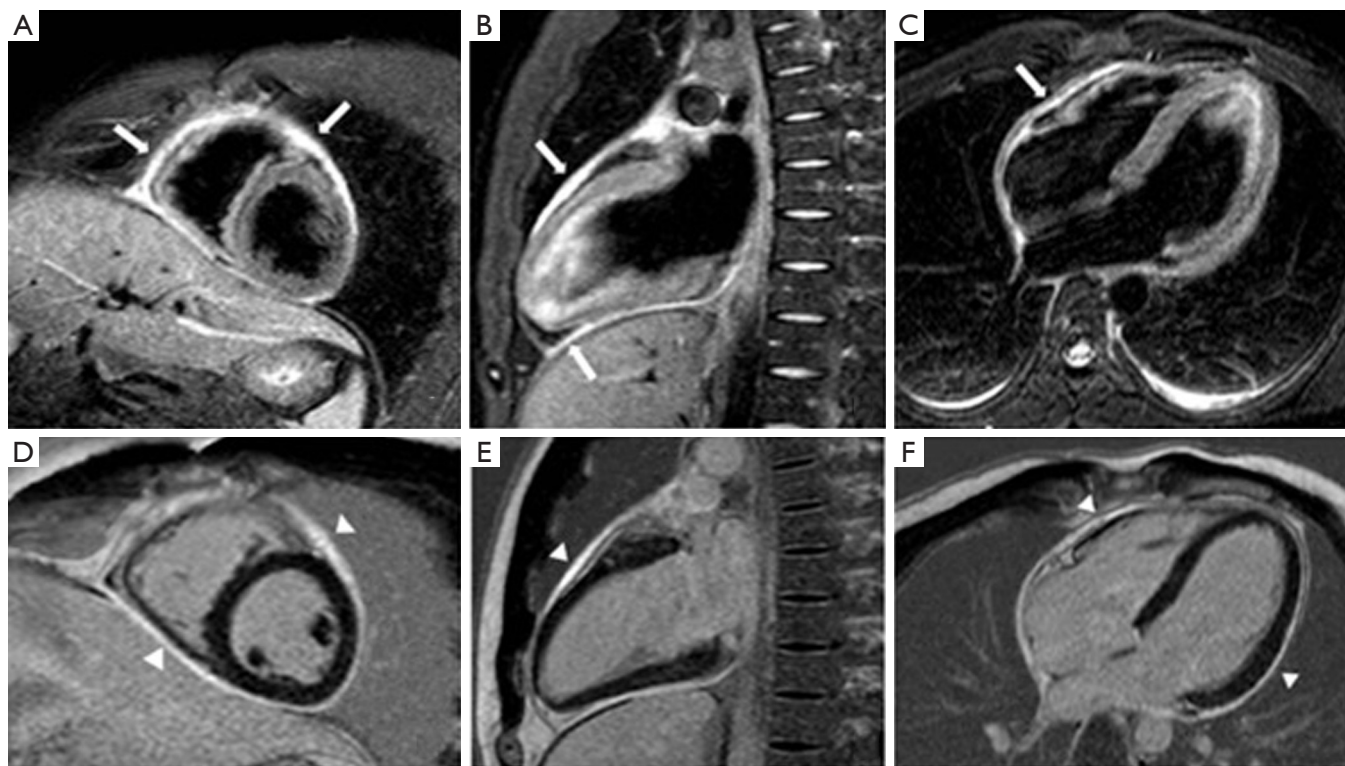


**Figure 11** Acute pericarditis. (A) Short-axis, (B) vertical long-axis, (C) horizontal long-axis T2-weighted short tau inversion-recovery spin-echo MR imaging show edema of the inflamed pericardial layers (arrows), (D) short-axis, (E) vertical long-axis, (F) horizontal long-axis late gadolinium-enhanced MR images show myocardial enhancement (arrowheads).

calcium within the pericardium is difficult to appreciate on CMR due to the signal loss in an already hypointense structure. Pericardial calcifications can also be visualised on CMR but CT imaging is preferred (53).

#### **Future direction**

Long acquisition times, ghosting artefacts, and irregular cardiac and respiratory motion limits the utility of CMR. Numerous technological advances are underway to overcome these barriers. The 3 and 7 T magnets provide better signal-to-noise ratio with improved spatial and



**Figure 12** Gradient pulse echo cine imaging using SSFP at 1.5 T and free-breathing technique to show constrictive physiology with flattening of the interventricular septum on deep inspiration (star).

temporal resolution, resulting in clearer images, but interferes more with EKG gating (62) and adjustments to radiofrequency pulses are required to reduce artefacts (16). Acoustic (phonocardiogram) gating has been previously proposed to improve image quality in patients with arrhythmias, but have not made promising results with 1.5 T magnets. With increasing EKG interference in 3 T and 7 T magnets, acoustic gating may provide an alternative in higher magnetic fields.

Cardiac motion gating is promising and its development is targeted at overcoming challenges in coronary MRA. Free-breathing respiratory-gated diaphragmatic navigation has been used to track the displacement of the right hemidiaphragm to indirectly predict the respiratory motion of the heart in a one-dimensional superior-inferior direction (63). This generates a narrow gating window at end expiration for image acquisition. This method reduces ghosting artefact but at the expense of prolong scanning time (64,65). Multiple advanced motion correction techniques using 2-, 3-dimensional self-navigation gating systems have been developed for image reconstruction (66-72). These techniques use low resolution 2D or 3D localizing images immediately before each image sequence to correct for beat-to-beat translational motion (73). Using 3D localization, compressed sensing and 3D SSFP, MRA can achieve resolution of  $1.2 \text{ mm}^3$  with shortened scanning time (69). Although these studies are small, they provide promising foundation for further developments in coronary MRA.

Hybrid PET/MR imaging have been explored in the research domain for its potential in providing both biochemical and anatomical assessment of coronary atherosclerosis, myocardial inflammation, infiltrative

diseases, and cardiac masses (74,75). Novel tracers including  $^{18}\text{F}$ -sodium fluoride and  $^{18}\text{F}$ -fluoro-deoxyglucose ( $^{18}\text{F}$  FDG) have been studied but further validations are required. Interventional CMR have been proposed but preliminary barriers include configuring the interventional suite with MR-conditional and MR-safe equipment (76).

## Conclusions

CMR has many advantages over conventional cardiac investigations, as a non-invasive measure of cardiac structure, function, tissue characterisation and metabolism, so great potential for expanding diagnostic and research indications in cardiology. CMR has become an instrumental tool for the evaluation and management of patients with structural heart disease, permitting an accurate diagnosis and reducing the need for invasive investigations. Challenges remain, including reducing the time of scan acquisitions and costs, to permit this technique to be routinely available worldwide.

## Acknowledgments

*Funding:* None.

## Footnote

*Provenance and Peer Review:* This article was commissioned by the Guest Editor (Ntobeko A. B. Ntusi) for the series “Cardiovascular Diseases in Low- and Middle-Income Countries” published in Cardiovascular Diagnosis and Therapy. The article was sent for external peer review organized by the Guest Editor and the editorial office.

*Conflicts of Interest:* All authors have completed the ICMJE uniform disclosure form (available at <http://dx.doi.org/10.21037/cdt.2019.06.02>). The series “Cardiovascular Diseases in Low- and Middle-Income Countries” was commissioned by the editorial office without any funding or sponsorship. The authors have no conflicts of interest to declare.

*Ethical Statement:* The authors are accountable for all aspects of the work in ensuring that questions related to the accuracy or integrity of any part of the work are appropriately investigated and resolved.

*Open Access Statement:* This is an Open Access article distributed in accordance with the Creative Commons Attribution-NonCommercial-NoDerivs 4.0 International License (CC BY-NC-ND 4.0), which permits the non-commercial replication and distribution of the article with the strict proviso that no changes or edits are made and the original work is properly cited (including links to both the formal publication through the relevant DOI and the license). See: <https://creativecommons.org/licenses/by-nc-nd/4.0/>.

## References

- Ridgway JP. Cardiovascular magnetic resonance physics for clinicians: part I. *J Cardiovasc Magn Reson* 2010;12:71.
- Moon JC, Messroghli DR, Kellman P, et al. Myocardial T1 mapping and extracellular volume quantification: a Society for Cardiovascular Magnetic Resonance (SCMR) and CMR Working Group of the European Society of Cardiology consensus statement. *J Cardiovasc Magn Reson* 2013;15:92.
- Messroghli DR, Moon JC, Ferreira VM, et al. Clinical recommendations for cardiovascular magnetic resonance mapping of T1, T2, T2\* and extracellular volume: A consensus statement by the Society for Cardiovascular Magnetic Resonance (SCMR) endorsed by the European Association for Cardiovascular Imaging (EACVI). *J Cardiovasc Magn Reson* 2017;19:75.
- Kim WY, Stuber M, Kissinger KV, et al. Impact of bulk cardiac motion on right coronary MR angiography and vessel wall imaging. *J Magn Reson Imaging* 2001;14:383-90.
- Larson AC, White RD, Laub G, et al. Self-gated cardiac cine MRI. *Magn Reson Med* 2004;51:93-102.
- Reeder SB, Faranesh AZ. Ultrafast pulse sequence techniques for cardiac magnetic resonance imaging. *Top Magn Reson Imaging* 2000;11:312-30.
- Gomori JM, Holland GI, Grossman RI, et al. Fat suppression by section-select gradient reversal on spin-echo MR imaging. Work in progress. *Radiology* 1988;168:493-5.
- Yilmaz A, Ferreira V, Klingel K, et al. Role of cardiovascular magnetic resonance imaging (CMR) in the diagnosis of acute and chronic myocarditis. *Heart Fail Rev* 2013;18:747-60.
- Kellman P, Arai AE. Cardiac imaging techniques for physicians: late enhancement. *J Magn Reson Imaging* 2012;36:529-42.
- Vöhringer M, Mahrholdt H, Yilmaz A, et al. Significance of late gadolinium enhancement in cardiovascular magnetic resonance imaging (CMR). *Herz* 2007;32:129-37.
- Syed IS, Glockner JF, Feng D, et al. Role of cardiac magnetic resonance imaging in the detection of cardiac amyloidosis. *JACC Cardiovasc Imaging* 2010;3:155-64.
- Ismail TF, Jabbour A, Gulati A, et al. Role of late gadolinium enhancement cardiovascular magnetic resonance in the risk stratification of hypertrophic cardiomyopathy. *Heart* 2014;100:1851-8.
- Kawel-Boehm N, Maceira A, Valsangiacomo-Buechel ER, et al. Normal values for cardiovascular magnetic resonance in adults and children. *J Cardiovasc Magn Reson* 2015;17:29.
- Almutairi HM, Boubertakh R, Miquel ME, et al. Myocardial deformation assessment using cardiovascular magnetic resonance-feature tracking technique. *Br J Radiol* 2017;90:20170072.
- Schulz-Menger J, Bluemke DA, Bremerich J, et al. Standardized image interpretation and post processing in cardiovascular magnetic resonance: Society for Cardiovascular Magnetic Resonance (SCMR) board of trustees task force on standardized post processing. *J Cardiovasc Magn Reson* 2013;15:35.
- Kramer CM, Barkhausen J, Flamm SD, et al. Standardized cardiovascular magnetic resonance (CMR) protocols 2013 update. *J Cardiovasc Magn Reson* 2013;15:91.
- Pothast S, Mitsumori L, Stanescu LA, et al. Measuring aortic diameter with different MR techniques: comparison of three-dimensional (3D) navigated steady-state free-precession (SSFP), 3D contrast-enhanced magnetic resonance angiography (CE-MRA), 2D T2 black blood, and 2D cine SSFP. *J Magn Reson Imaging* 2010;31:177-84.
- Hartung MP, Grist TM, Francois CJ. Magnetic resonance angiography: current status and future directions. *J Cardiovasc Magn Reson* 2011;13:19.
- Kim WY, Danias PG, Stuber M, et al. Coronary magnetic resonance angiography for the detection of coronary stenoses. *N Engl J Med* 2001;345:1863-9.
- Prasad SK, Lyne J, Chai P, et al. Role of CMR in assessment of myocardial perfusion. *Eur Radiol* 2005;15 Suppl 2:B42-7.
- Greenwood JP, Maredia N, Younger JF, et al. Cardiovascular magnetic resonance and single-photon emission computed tomography for diagnosis of coronary heart disease (CE-MARC): a prospective trial. *Lancet* 2012;379:453-60.
- Hendel RC, Friedrich MG, Schulz-Menger J, et al. CMR First-Pass Perfusion for Suspected Inducible Myocardial

- Ischemia. *JACC Cardiovasc Imaging* 2016;9:1338-48.
23. Tezuka D, Kosuge H, Terashima M, et al. Myocardial perfusion reserve quantified by cardiac magnetic resonance imaging is associated with late gadolinium enhancement in hypertrophic cardiomyopathy. *Heart Vessels* 2018;33:513-20.
  24. Lockie T, Ishida M, Perera D, et al. High-resolution magnetic resonance myocardial perfusion imaging at 3.0-Tesla to detect hemodynamically significant coronary stenoses as determined by fractional flow reserve. *J Am Coll Cardiol* 2011;57:70-5.
  25. Salerno M, Sharif B, Arheden H, et al. Recent Advances in Cardiovascular Magnetic Resonance: Techniques and Applications. *Circ Cardiovasc Imaging*, 2017;10. doi: 10.1161/CIRCIMAGING.116.003951.
  26. Greenwood JP, Ripley DP, Berry C, et al. Effect of Care Guided by Cardiovascular Magnetic Resonance, Myocardial Perfusion Scintigraphy, or NICE Guidelines on Subsequent Unnecessary Angiography Rates: The CE-MARC 2 Randomized Clinical Trial. *JAMA* 2016;316:1051-60.
  27. Ripley DP, Brown JM, Everett CC, et al. Rationale and design of the Clinical Evaluation of Magnetic Resonance Imaging in Coronary heart disease 2 trial (CE-MARC 2): a prospective, multicenter, randomized trial of diagnostic strategies in suspected coronary heart disease. *Am Heart J* 2015;169:17-24.e1.
  28. Schwitter J, Wacker CM, Wilke N, et al. MR-IMPACT II: Magnetic Resonance Imaging for Myocardial Perfusion Assessment in Coronary artery disease Trial: perfusion-cardiac magnetic resonance vs. single-photon emission computed tomography for the detection of coronary artery disease: a comparative multicentre, multivendor trial. *Eur Heart J* 2013;34:775-81.
  29. Romano S, Romer B, Evans K, et al. Prognostic Implications of Blunted Feature-Tracking Global Longitudinal Strain During Vasodilator Cardiovascular Magnetic Resonance Stress Imaging. *JACC Cardiovasc Imaging* 2020;13:58-65.
  30. Hudsmith LE, Petersen SE, Tyler DJ, et al. Determination of cardiac volumes and mass with FLASH and SSFP cine sequences at 1.5 vs. 3 Tesla: a validation study. *J Magn Reson Imaging* 2006;24:312-8.
  31. Patel AR, Kramer CM. Role of Cardiac Magnetic Resonance in the Diagnosis and Prognosis of Nonischemic Cardiomyopathy. *JACC Cardiovasc Imaging* 2017;10:1180-93.
  32. Pinto YM, Elliott PM, Arbustini E, et al. Proposal for a revised definition of dilated cardiomyopathy, hypokinetic non-dilated cardiomyopathy, and its implications for clinical practice: a position statement of the ESC working group on myocardial and pericardial diseases. *Eur Heart J* 2016;37:1850-8.
  33. Brenes JC, Doltra A, Prat S. Cardiac magnetic resonance imaging in the evaluation of patients with hypertrophic cardiomyopathy. *Glob Cardiol Sci Pract* 2018;2018:22.
  34. Tang CX, Petersen SE, Sanghvi MM, et al. Cardiovascular magnetic resonance imaging for amyloidosis: The state-of-the-art. *Trends Cardiovasc Med* 2019;29:83-94.
  35. Di Bella G, Pizzino F, Minutoli F, et al. The mosaic of the cardiac amyloidosis diagnosis: role of imaging in subtypes and stages of the disease. *Eur Heart J Cardiovasc Imaging* 2014;15:1307-15.
  36. Bennett RG, Haqqani HM, Berrueto A, et al. Arrhythmogenic Cardiomyopathy in 2018-2019: ARVC/ALVC or Both? *Heart Lung Circ* 2019;28:164-77.
  37. Marcus FI, McKenna WJ, Sherrill D, et al. Diagnosis of arrhythmogenic right ventricular cardiomyopathy/dysplasia: proposed modification of the task force criteria. *Circulation* 2010;121:1533-41.
  38. Eitel I, Friedrich MG. T2-weighted cardiovascular magnetic resonance in acute cardiac disease. *J Cardiovasc Magn Reson* 2011;13:13.
  39. Myerson SG, Holloway CJ, Francis JM, et al. Cardiovascular magnetic resonance (CMR)--an update and review. *Prog Nucl Magn Reson Spectrosc* 2011;59:213-22.
  40. Baritussio A, Scatteia A, Bucciarelli-Ducci C. Role of cardiovascular magnetic resonance in acute and chronic ischemic heart disease. *Int J Cardiovasc Imaging* 2018;34:67-80.
  41. de Waha S, Eitel I, Desch S, et al. Prognosis after ST-elevation myocardial infarction: a study on cardiac magnetic resonance imaging versus clinical routine. *Trials* 2014;15:249.
  42. Fernández-Friera L, Garcia-Ruiz JM, Garcia-Alvarez A, et al. Accuracy of Area at Risk Quantification by Cardiac Magnetic Resonance According to the Myocardial Infarction Territory. *Rev Esp Cardiol (Engl Ed)* 2017;70:323-30.
  43. van Kranenburg M, Magro M, Thiele H, et al. Prognostic value of microvascular obstruction and infarct size, as measured by CMR in STEMI patients. *JACC Cardiovasc Imaging* 2014;7:930-9.
  44. Hamirani YS, Wong A, Kramer CM, et al. Effect of microvascular obstruction and intramyocardial hemorrhage by CMR on LV remodeling and outcomes after myocardial

- infarction: a systematic review and meta-analysis. *JACC Cardiovasc Imaging* 2014;7:940-52.
45. Dweck MR, Williams MC, Moss AJ, et al. Computed Tomography and Cardiac Magnetic Resonance in Ischemic Heart Disease. *J Am Coll Cardiol* 2016;68:2201-16.
  46. Kim RJ, Wu E, Rafael A, et al. The use of contrast-enhanced magnetic resonance imaging to identify reversible myocardial dysfunction. *N Engl J Med* 2000;343:1445-53.
  47. Gerber BL, Darchis J, le Polain de Waroux JB, et al. Relationship between transmural extent of necrosis and quantitative recovery of regional strains after revascularization. *JACC Cardiovasc Imaging* 2010;3:720-30.
  48. Daly C, Kwong RY. Cardiac MRI for myocardial ischemia. *Methodist Debaquey Cardiovasc J* 2013;9:123-31.
  49. Greenwood JP, Motwani M, Maredia N, et al. Comparison of cardiovascular magnetic resonance and single-photon emission computed tomography in women with suspected coronary artery disease from the Clinical Evaluation of Magnetic Resonance Imaging in Coronary Heart Disease (CE-MARC) Trial. *Circulation* 2014;129:1129-38.
  50. Aquaro GD, Di Bella G, Castelletti S, et al. Clinical recommendations of cardiac magnetic resonance, Part I: ischemic and valvular heart disease: a position paper of the working group 'Applicazioni della Risonanza Magnetica' of the Italian Society of Cardiology. *J Cardiovasc Med (Hagerstown)* 2017;18:197-208.
  51. Mathew RC, Loffler AI, Salerno M. Role of Cardiac Magnetic Resonance Imaging in Valvular Heart Disease: Diagnosis, Assessment, and Management. *Curr Cardiol Rep* 2018;20:119.
  52. Garcia J, Barker AJ, Markl M. The Role of Imaging of Flow Patterns by 4D Flow MRI in Aortic Stenosis. *JACC Cardiovasc Imaging* 2019;12:252-66.
  53. Bogaert J, Francone M. Pericardial disease: value of CT and MR imaging. *Radiology* 2013;267:340-56.
  54. Srichai MB. CMR imaging in constrictive pericarditis: is seeing believing? *JACC Cardiovasc Imaging* 2011;4:1192-4.
  55. Adler Y, Charron P, Imazio M, et al. 2015 ESC Guidelines for the diagnosis and management of pericardial diseases. Task Force for the Diagnosis and Management of Pericardial Diseases of the European Society of Cardiology (ESC). *G Ital Cardiol (Rome)* 2015;16:702-38.
  56. Kligerman S. Imaging of Pericardial Disease. *Radiol Clin North Am* 2019;57:179-99.
  57. Young PM, Glockner JF, Williamson EE, et al. MR imaging findings in 76 consecutive surgically proven cases of pericardial disease with CT and pathologic correlation. *Int J Cardiovasc Imaging* 2012;28:1099-109.
  58. Cummings KW, Green D, Johnson WR, et al. Imaging of Pericardial Diseases. *Semin Ultrasound CT MR* 2016;37:238-54.
  59. Feng D, Glockner J, Kim K, et al. Cardiac magnetic resonance imaging pericardial late gadolinium enhancement and elevated inflammatory markers can predict the reversibility of constrictive pericarditis after antiinflammatory medical therapy: a pilot study. *Circulation* 2011;124:1830-7.
  60. Bogaert J, Francone M. Cardiovascular magnetic resonance in pericardial diseases. *J Cardiovasc Magn Reson* 2009;11:14.
  61. Klein AL, Abbara S, Agler DA, et al. American Society of Echocardiography clinical recommendations for multimodality cardiovascular imaging of patients with pericardial disease: endorsed by the Society for Cardiovascular Magnetic Resonance and Society of Cardiovascular Computed Tomography. *J Am Soc Echocardiogr* 2013;26:965-1012.e15.
  62. Frauenrath T, Hezel F, Renz W, et al. Acoustic cardiac triggering: a practical solution for synchronization and gating of cardiovascular magnetic resonance at 7 Tesla. *J Cardiovasc Magn Reson* 2010;12:67.
  63. McLeish K, Hill DL, Atkinson D, et al. A study of the motion and deformation of the heart due to respiration. *IEEE Trans Med Imaging* 2002;21:1142-50.
  64. Wang Y, Riederer SJ, Ehman RL. Respiratory motion of the heart: kinematics and the implications for the spatial resolution in coronary imaging. *Magn Reson Med* 1995;33:713-9.
  65. Ehman RL, Felmlee JP. Adaptive technique for high-definition MR imaging of moving structures. *Radiology* 1989;173:255-63.
  66. Stehning C, Bornert P, Nehrke K, et al. Free-breathing whole-heart coronary MRA with 3D radial SSFP and self-navigated image reconstruction. *Magn Reson Med* 2005;54:476-80.
  67. Pang J, Bhat H, Sharif B, et al. Whole-heart coronary MRA with 100% respiratory gating efficiency: self-navigated three-dimensional retrospective image-based motion correction (TRIM). *Magn Reson Med* 2014;71:67-74.
  68. Henningson, M, Koken P, Stehning C, et al. Whole-heart coronary MR angiography with 2D self-navigated image reconstruction. *Magn Reson Med* 2012;67:437-45.
  69. Moghari MH, Annese D, Geva T, et al. Three-dimensional

- heart locator and compressed sensing for whole-heart MR angiography. *Magn Reson Med* 2016;75:2086-93.
70. Addy NO, Ingle RR, Luo J, et al. 3D image-based navigators for coronary MR angiography. *Magn Reson Med* 2017;77:1874-83.
71. Zitzelsberger, T, Krumm P, Hornung A, et al. Multi-phase coronary magnetic resonance angiography improves delineation of coronary arteries. *Acta Radiol* 2019;60:1422-9.
72. Henningsson M, Shome J, Bratis K, et al. Diagnostic performance of image navigated coronary CMR angiography in patients with coronary artery disease. *J Cardiovasc Magn Reson* 2017;19:68.
73. Correia T, Ginami G, Cruz G, et al. Optimized respiratory-resolved motion-compensated 3D Cartesian coronary MR angiography. *Magn Reson Med* 2018;80:2618-29.
74. Wurster T, Landmesser U, Engel LC, et al. Coronary Vessel Wall Imaging: State of the Art and Future Directions. *Curr Cardiovasc Imaging Rep* 2019;12:16.
75. Nensa F, Poeppel TD, Beiderwellen K, et al. Hybrid PET/MR imaging of the heart: feasibility and initial results. *Radiology* 2013;268:366-73.
76. Rogers T, Lederman RJ. Interventional CMR: Clinical applications and future directions. *Curr Cardiol Rep* 2015;17:31.

**Cite this article as:** Situ Y, Birch SCM, Moreyra C, Holloway CJ. Cardiovascular magnetic resonance imaging for structural heart disease. *Cardiovasc Diagn Ther* 2020;10(2):361-375. doi: 10.21037/cdt.2019.06.02